Solitary current-density patterns in thin ZnS:Mn films

S. Zuccaro, F.-J. Niedernostheide, B. Kukuk, M. Strych, and H.-G. Purwins
Institute of Applied Physics,University of Münster, Corrensstrasse 2 - 4, 48149 Münster, Germany
(Received 7 September 1999)

We experimentally investigate pattern formation phenomena in the electroluminescence of ac-driven ZnS:Mn thin films. Under suitable driving conditions, certain samples show a broad spectrum of patterns, which ranges from stationary filamentary distributions to traveling fronts and pulses. We present a survey of the bifurcation scenarios, choosing the frequency and amplitude of the driving voltage as bifurcation parameters. Moreover, we investigate the influence of the temperature on the dissipative current and pattern formation. The experimental results are used to identify activating and inhibiting processes, and a pattern formation mechanism based on autocatalysis and lateral inhibition is suggested.

PACS number(s): 47.54.+r, 78.60.Fi, 05.70.Ln, 72.20.Ht

I. INTRODUCTION

The spontaneous formation of spatial patterns is a widespread phenomenon in nonlinear dissipative systems. In many cases it has been shown that the generation of self-organized patterns is based on processes involving local autocatalysis and lateral inhibition. Well-known examples are chemical (e.g., Ref. [1,2]) or biological (e.g., Ref. [3,4]) systems, which can often be described in terms of two-component reaction-diffusion equations with an activator enhancing the generation of one or both variables, and an inhibitor suppressing the production of both components. In several semiconductor structures [5–11] and gas discharge systems [12–14] the spontaneous formation of inhomogeneous current-density distributions has likewise been successfully described in the framework of local autocatalysis and lateral inhibition. Moreover, systems with more than one activating and one inhibiting component have generated increasing interest recently, since in this case additional patterns can be stabilized [16–18].

Among the semiconductor systems revealing pattern formation, particularly rich scenarios are shown by thin ZnS:Mn films with a doping concentration of the order of a few mol %, in which the Mn atoms act as light-emitting centers when they are impact excited by the current transporting electrons. In addition to filamentary current-density distributions [19,20] and expanding high current domains [21–23], patterns that are often found in semiconductor systems, phenomena that are characteristic of excitable media, like spiral waves and target patterns [24–26] have also been observed. Although the similarity between the patterns observed in ZnS:Mn films and structures in reaction-diffusion systems has already been pointed out in earlier work [15,25,26,23], there is only an incomplete understanding of the physical processes underlying the observed phenomena.

In this paper we propose an interpretation of pattern formation in ZnS:Mn films within the framework of autocatalysis and lateral inhibition. To this end, we investigate the influence of the samples' physical properties and operating conditions on the light-density distribution and identify suitable activating and inhibiting mechanisms.

II. EXPERIMENTAL SETUP

The samples under investigation consist of an electroluminescent, Mn-doped layer of ZnS sandwiched between two insulating layers. Two electrodes made of indium tin oxide (ITO), a transparent, conducting oxide, and aluminum complete the device (Fig. 1). The insulating layer deposited on the ITO electrode consists of AlO_xN_y, while the second one is a sandwich structure of AlO_xN_y and $BaTa_2O_6$. The thickness of the insulators is about 200 nm. The active semiconductor layer with a thickness between 300 and 500 nm was grown by multisource deposition. The final top Al contacts with a diameter of 1.5 mm define the active area of the samples.

The samples are ac driven with amplitudes between 70 V and 200 V and frequencies of up to 300 kHz, so that the flow of dissipative current occurs in short pulses, one for each half cycle of the driving voltage. The light-density distribution is detected through the transparent ITO layer with an intensified charge-coupled device camera mounted on a long-working-distance microscope. The temporal resolution of the video camera employed is 20 ms. Time resolved measurements of the samples' global luminous intensity are carried out with an SFH 100 photodiode, while the charge trans-

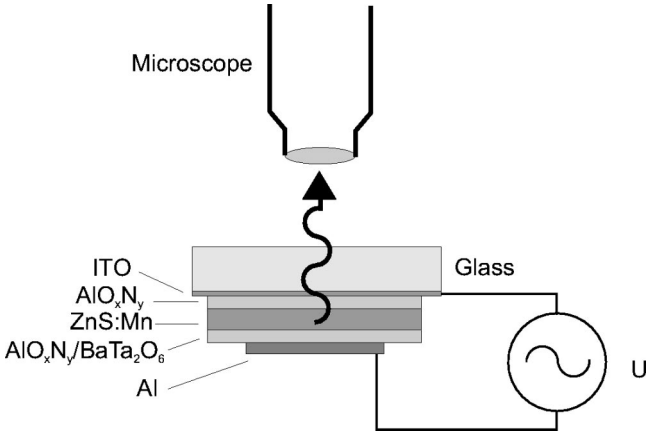

FIG. 1. Cross sectional structure of a ZnS:Mn thin film device. The thin film stack is about 1 μm thick, while the lateral extension is 1.5 mm.

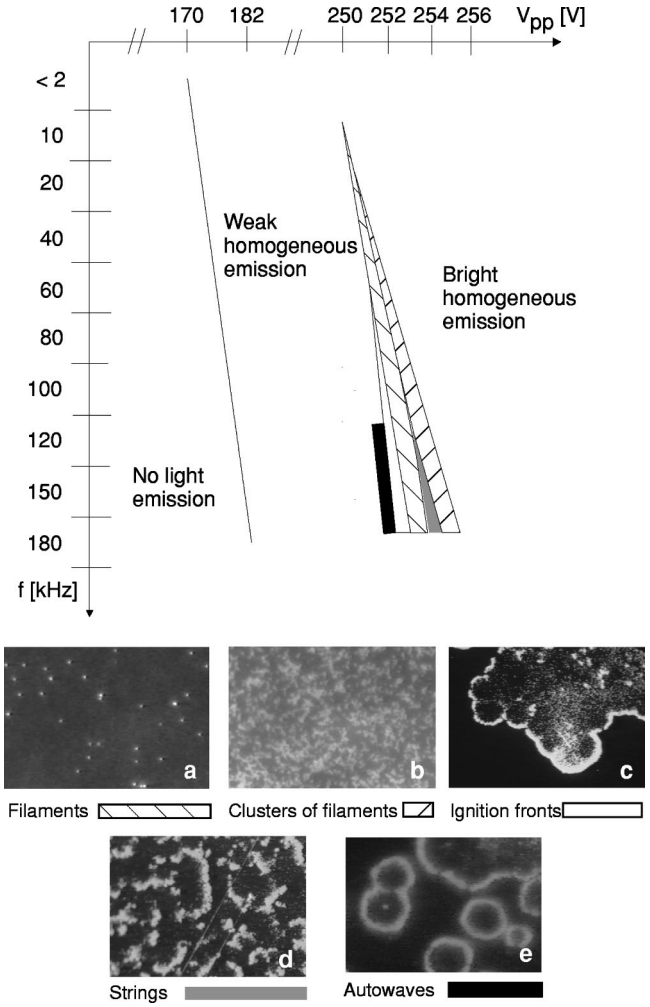

FIG. 2. Bifurcation scenarios in a sample with $c_{Mn}=0.8$ mol %. The measurement was made at room temperature. (a) Stationary filaments, (b) clusters of filaments, (c) ignition fronts, (d) luminescent strings, and (e) autowaves ignited by suddenly cooling the sample by 20 °C. Image size: 180×130 μm^2 (a),(b), 400×280 μm^2 (c)–(e).

ferred through the phosphor layer in every half cycle of the driving voltage is measured by the Sawyer-Tower method [27], in which a sense capacitor connected in series to the sample integrates the total current.

Current conduction in the semiconductor layer is initiated by applying a field on the order of 1 MV/cm, so that electrons trapped in interfacial states at the insulator-semiconductor boundaries and, to a minor extent, in donor-like centers in the bulk of the semiconductor film [28,29] can tunnel into the conduction band of the ZnS. The light-emitting Mn centers are impact excited by the conduction electrons; the relaxation back to the ground state is coupled to the emission of light whose spectrally resolved intensity shows a maximum at about 585 nm, giving rise to the characteristic yellow-orange electroluminescence.

The electric field at which current conduction takes place can be derived from the film thickness and the intersection with the voltage axis of the tangent line to the charge-voltage characteristic in the part where the ZnS layer is conducting [27], while the concentration of the Mn dopant is determined from the time constant of the afterglow decay of the samples under pulsed excitation according to Ref. [30].

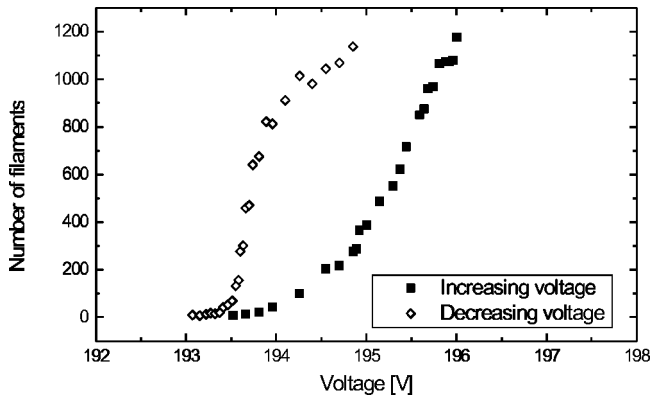

FIG. 3. Number of filaments as a function of the driving amplitude on an area of 158×150 μm^2. Parameters: sample no. 1, $f=5.32$ kHz.

III. PATTERN FORMATION PHENOMENA

Inhomogeneous light-density distributions can be observed in samples with a minimum ZnS layer thickness of about 300 nm and Mn concentrations below ca. 2 mol %. The two basic pattern classes found are stationary distributions of microfilaments and traveling waves. Typical examples for the structures are shown in Fig. 2, along with a bifurcation scenario including both the stationary and dynamical patterns for a sample with a Mn concentration of 0.8 mol %.

Filamentary current distributions can be observed in all devices satisfying these requirements at driving frequencies higher than a few kHz. When the voltage is increased starting from values at which no flow of dissipative current occurs, uniform emission of yellow light sets in at a threshold voltage amplitude that depends on the thickness of the layers and has a peak-to-peak value of $V_{pp}=170$ V for this sample; this corresponds to a field of about 1.6 MV/cm in the semiconductor layer. However, at a second peak-to-peak voltage threshold of 250 V isolated bright spots with a diameter of about 1 μm appear on the dim electroluminescence background at randomly distributed positions. Upon increasing the applied voltage, the density of these spots increases continuously; eventually, they merge together to form extended regions with high electroluminescence (EL) emission, until the whole sample is switched into the high intensity mode.

It has been known since the work of Rühle, Marrello, and Onton [19] that filamentary conduction occurs in samples showing a hysteresis in the brightness-voltage characteristic of both the whole device and a single filament. For a quantitative characterization of stationary multifilamentary patterns, the number and mean diameter of the filaments have been evaluated as a function of the applied voltage amplitude. The number of filaments on the domain as a function of the voltage shows, as expected, a correlation between the hysteresis behavior of the filament density and the global luminous intensity of the sample (Fig. 3). An evaluation of the mean filament diameter as a function of the number of filaments on the analyzed domain shows that the growth process proceeds in two phases: near the threshold voltage, or at

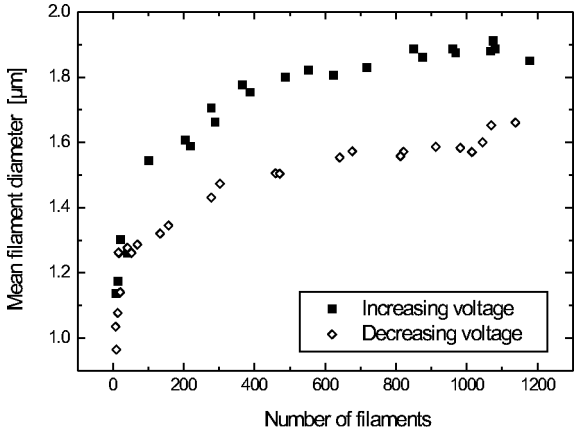

FIG. 4. Averaged filament diameter as a function of the number of filaments. Parameters as in Fig. 4.

low filament density, one observes a strong increase in the diameter, so that the expansion of the filaments significantly contributes to the increase in global brightness; at higher densities, the mean diameter tends to saturate at a value of about 1.9 μm for the images investigated. When the number of filaments is decreased, however, their mean diameter already shrinks at the beginning of the back branch of the hysteresis loop, stays constant at a value of about 1.5 μm, and decreases significantly only at low voltages (Fig. 4).

The second class of patterns found in the samples investigated are traveling waves. They, too, require a minimum ZnS layer thickness of about 300 nm, but exist in a narrower parameter range than stationary filaments. They can be observed only in samples with a doping concentration below about 1 mol % and at frequencies one order of magnitude higher than those necessary for the spots. Starting from low driving amplitudes at a high enough frequency, again a homogeneous background electroluminescence sets in at first, until at a certain threshold voltage line-shaped luminescent strings are ignited at different locations on the sample (Fig. 2). Their linear extent typically lies in the range between 500 and 1000 μm, and after having traveled over distances of up to 1 mm, they extinguish either spontaneously or when reaching the sample boundaries, leaving behind both stationary filaments and smaller strings. As they switch the sample into a condition of higher activity, we call them ''ignition fronts.'' The smaller strings are continuously generated at randomly distributed locations and have typical lengths of up to 20 or 30 μm and velocities of about $20-30$ μm/s (Fig. 2). When their length reaches the value of about 30 μm they decay into smaller fragments which, in turn, propagate away from the generation center and begin to expand.

While strings originating spontaneously at room temperature and at constant driving parameters show a strong tendency to decay into short fragments, ring-shaped waves ignited by, e.g., sudden temperature, frequency, or voltage variations, are more stable against spontaneous decay and show several features typical of solitary waves in excitable media (Fig. 5).

When two waves collide, their intensities do not superimpose, as is the case for linear waves, but annihilate, leaving behind the sample in a low intensity state. Another characteristic property of excitable media, that is to say, the existence of a refractory condition after the relaxation back to the

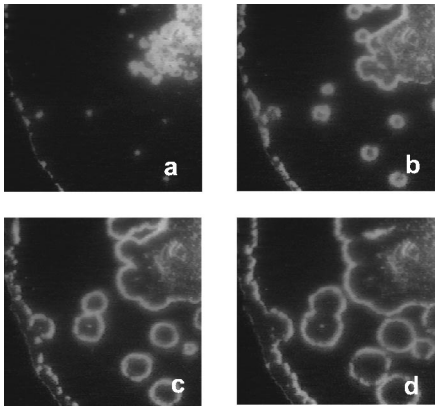

FIG. 5. Expansion of ring-shaped, solitary waves. The waves were ignited by suddenly cooling down the sample to about 273 K. Parameters: sample no. 2, $f=190$ kHz, $V_{pp}=270$ V, image size 450×440 μm^2, time between subsequent pictures 100 ms.

quiescent state, could be directly observed by igniting pulses twice with a temporal delay of 1 s (Fig. 6). New pulses are ignited only at locations that have not been reached yet by the first ring waves; the regions within the rings ignited first remain in the low intensity state nearly 1 s longer than the rest of the sample. It is evident from Fig. 5 that ring waves are often ignited at inhomogeneities in the layers. The bright spot in the upper, right corner, for example stems from the contact probe connected to the Al dot and acts as a preferred generation center for pulses. Isolated filaments can trigger the creation of pulses as well, as can be seen from the left part of the figure.

IV. DISCUSSION OF ACTIVATING AND INHIBITING MECHANISMS

The similarity between the pattern formation phenomena in thin ZnS:Mn films and those known from systems with local autocatalysis and lateral inhibition motivates our search for an explanation of the observed phenomena within this framework. A particularly intriguing question is the existence of different length scales concerning the dimensions of the stationary and traveling patterns, as well as of different time scales in the dynamics of the dissipative current, on the

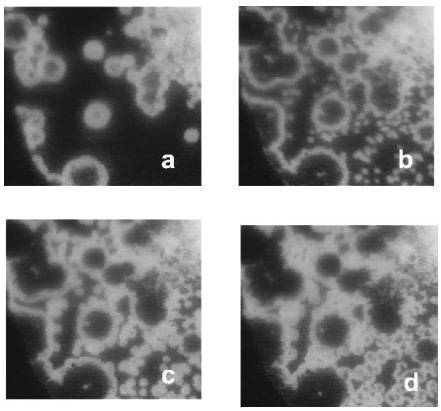

FIG. 6. Refractory state of the medium after the passage of high-current pulses. Parameters: sample no. 2, $f=180$ kHz, $V_{pp}=264$ V, image size 450×440 μm^2, time between subsequent pictures 60 ms.

one hand, and of the patterns, on the other.

There are two important activating processes working on different time scales. The first one is based on avalanche electron multiplication by impact ionization of deep centers [11] and/or by band-to-band impact ionization at high electric fields accompanied by a positive feedback loop: as suggested in Ref. [31], the holes are captured nearly instantaneously by deep hole traps which are related to the Mn doping, while the electrons drift to the momentary anode and are captured by the interface traps. The positively charged traps cause a field redistribution in such a way that the barrier width for electrons located at the interface states of the semiconductor-insulator interface near the momentary cathode decreases; this leads to an enhanced tunnel injection of these electrons into the conduction band of the ZnS, which, in turn, causes an increase in dissipative current and local EL emission.

The sharp thresholdlike dependence of pattern formation on the voltage amplitude observed in Fig. 2 can be explained by the strong dependence of impact ionization processes on the electric field. Moreover, an evaluation of the charge-voltage characteristic of our EL structures shows that in the samples displaying pattern formation phenomena the electric fields lie between 1.6 and 2.2 MV/cm, values at which the impact ionization coefficient in ZnS becomes significant [32].

The charges trapped in the interfaces are responsible for a second, slower activating process: while tunnel emission of carriers and impact ionization are effects taking place on a time scale several orders of magnitude smaller than the duration of one half cycle of the driving voltage (which is at least 5 μs in our samples), the dynamical patterns evolve on a slower time scale in the millisecond range, so that a process which ensures the continuation of current reinforcement over many cycles is necessary. A mechanism that produces this ''memory effect'' is provided by the interface charges, because a patterned current density during the current flow phase will cause a corresponding spatial modulation in the charge density collected at the anodic interface, which will, in turn, inject a modulated current into the ZnS layer during the next half cycle of the driving voltage, when it will act as the cathodic interface. In order to estimate the maximum period up to which the interface charges have a significant influence on the breakdown behavior in the subsequent half period, the following experiment has been performed. Triangular voltage pulses were applied to the sample with two subsequent pulses showing the same polarity (Fig. 8). During the first pulse of a given polarity, one always observes a dissipative current peak superimposed on the displacement current, which has a rectangular shape since it is proportional to the time derivative of the triangular voltage wave form; during the second pulse, this happens only at low frequencies. The time interval after which a dissipative current can be found in the second pulse typically lies between 10 ms and 100 ms, depending on the sample. So part of the charge stored in the interfaces, which creates an internal field opposite to the externally applied one, decays over time intervals in the 10 ms range. It follows from these considerations that the memory effect of the interfaces is more effective at higher frequencies, so that the activating current reinforcement is enhanced, providing an explanation for the second striking feature of the V_{pp}-f diagram, namely, the necessity of applying high frequencies to observe patterned EL distributions.

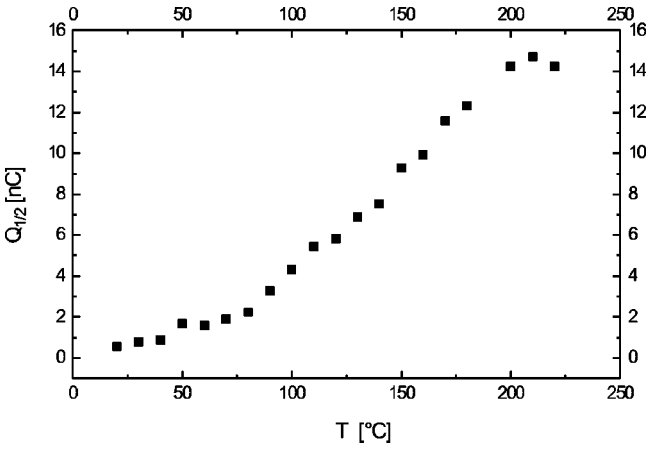

FIG. 7. Charge transferred during one half cycle of the driving voltage as a function of temperature. The temperature was raised at a rate of 0.35 K/s.

Another effect of an increase of the driving frequency is a stronger heating of the sample, since the dissipated power increases as a consequence. To investigate the influence of this effect on current flow, we analyzed the charge-voltage characteristic at different temperatures. The samples were initially biased at voltages just below the threshold that initiates current conduction and then heated at a constant rate of at most 1 K/s. Typical results obtained at a heating rate of 0.35 K/s are plotted in Fig. 7. One observes a continuous increase in the transferred charge as the temperature is raised. An observation of the filamentary distributions upon heating the sample is in accordance with this scenario: at temperatures of about $40-60\,^{\circ}\mathrm{C}$ the boundaries of the filaments become blurred, while the background electroluminescence increases; at temperatures between $60\,^{\circ}\mathrm{C}$ and $100\,^{\circ}\mathrm{C}$, depending on the properties of the samples, the filaments appear to dissolve in the background.

These results can be explained, if deep trap levels in the band gap are taken into account. Depending on the applied film preparation techniques and the annealing procedure, the concentration of these centers is on the order of 10^{16} to 10^{19} cm^{-3} with energy levels of up to 1 eV below the conduction band edge [29,33]. While band gap states at this depth should not be significantly thermally depopulated in a flat-band situation at room temperature, phonon assisted tunneling due to the field induced band bending is a reasonable explanation for the observed phenomenon [34]. It is important to note that a continuous increase of the temperature also takes place as a consequence of Joule heating whenever the current density increases with time. Thus, current and temperature growth can reinforce each other.

In the same way as the stored charge at the cathodic interface increases the electric field at the beginning of each half period, the negative charge accumulating at the anodic interface during the flow of dissipative current counteracts the charge transfer, providing an effective inhibiting mechanism at the end of the current flow phase. The evolution and stabilization of stationary filamentary patterns can be understood as an interplay between these autocatalytic and inhib-

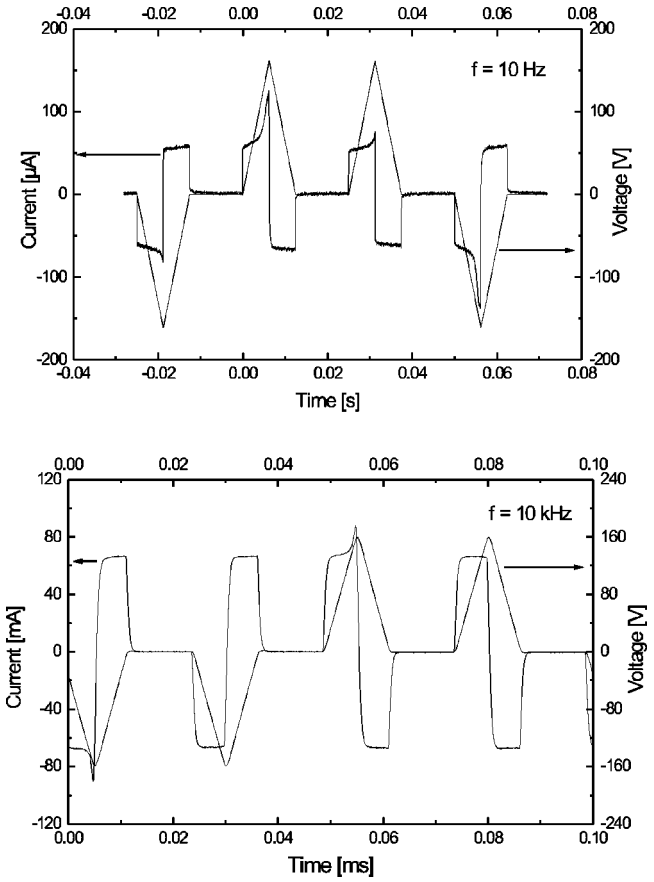

FIG. 8. Applied triangular voltage pulses and total current at different frequencies. A dissipative current peak at the second pulse of a given polarity is found only at low frequencies (see text).

iting processes, whereby the latter sets in with a certain temporal delay with respect to the former. The mechanism considered in the following in more detail is similar to a scenario that has recently been proposed and confirmed by numerical simulations of a fluid model to explain filamentary current flow in ac-driven dielectric barrier gas discharges [13,14].

In order to see how filaments may be stabilized, imagine a stationary uniform state and consider the evolution of a small positive fluctuation of, e.g., the electron distribution in the ZnS film. For sufficiently large electric fields, impact ionization processes and the increased tunnel injection from interfacial states lead to an amplification of the local electron concentration, eventually resulting in an inhomogeneous charge distribution at the anodic semiconductor-insulator interface. Because the electric field distribution at the beginning of the next half cycle has its maximum at the location corresponding to the greatest interfacial charge density, tunnel injection and impact ionization will start first at the position of the maximum in the now cathodic interfacial charge density. The decrease of the charge density at the center of the fluctuation leads to a transverse field near the cathode, focusing the electrons near the center of the fluctuation. Thus, there is a self-focusing of the transferred charge at the beginning of each charge-transfer cycle, leading to a strong increase of current flow in the center of the evolving filament. In the course of charge transfer the electrons are collected at the anodic interface, leading to the evolution of a counterfield with a maximum again at the center of the original fluctuation. Due to the self-focusing property near the cathode the maximum of the counterfield rises faster than in the uniform case, and, consequently, the charges collected at the anodic interface will also spread faster in the direction transverse to the main current flow. By that mechanism the counterfield rapidly becomes effective also at a certain distance from the center of the evolving filament, prohibiting its transverse spreading. So it acts as a fast inhibitor, capable of stabilizing a stationary filament.

With increasing frequency the stability of stationary filaments becomes weaker because the time delay between the rising of the tunnel injection at the center of the filament and outside the filament decreases. Consequently, the self-focusing behavior of the charge transfer during the first stage is less pronounced and the lateral inhibition in the second stage is weakened, providing better conditions for the evolution of dynamic structures.

V. SUMMARY

In this paper, we experimentally investigated pattern formation phenomena in ac-driven ZnS:Mn films. We analyzed the influence of the driving amplitude, frequency, and sample temperature on the pattern formation in the transverse electroluminescence distribution. It is suggested that the evolution of stationary filaments and dynamical structures is determined by the interplay between autocatalytic and inhibiting processes, whose temporal competition influences the tangential electric fields near the interfaces, and thus determines the lateral charge spreading.

ACKNOWLEDGMENTS

The authors would like to thank the Heinrich-Hertz-Institut für Nachrichtentechnik Berlin GmbH, AG Elektrolumineszenz, for kindly supplying some of the samples investigated. We are indebted to Dr. G. Spiekermann and Dr. E. Ammelt for the use of their image processing systems. Financial support by the Deutsche Forschungsgemeinschaft is gratefully acknowledged.

[1] *Chemical Waves and Patterns*, edited by R. Kapral and K. Showalter (Kluwer, Dordrecht, 1995).

[2] A. S. Mikhailov, *Foundations of Synergetics I*, 2nd ed. (Springer, Berlin, 1994).

[3] J. D. Murray, *Mathematical Biology*, 2nd ed. (Springer, Berlin, 1993).

[4] *Modelling the Dynamics of Biological Systems*, edited by E. Mosekilde and O.G. Mouritsen (Springer, Berlin, 1995).

[5] B. S. Kerner and V. V. Osipov, *Autosolitons* (Kluwer, Dordrecht, 1994).

[6] A. V. Gorbatyuk and P. B. Rodin, in *Proceedings of the 6th International Symposium on Power Semiconductor Devices*

Davos, 1994, edited by W. Fichtner, A. A. Jacklin, and D. Aemmer (Hartung-Gorre Verlag, Konstanz, 1994), p. 237.
[7] F.-J. Niedernostheide, B. S. Kerner, and H.-G. Purwins, Phys. Rev. B **46**, 7559 (1992).
[8] F.-J. Niedernostheide, M. Or-Guil, M. Kleinkes, and H.-G. Purwins, Phys. Rev. E **55**, 4107 (1997).
[9] M. Meixner, P. Rodin, and E. Schöll, Phys. Rev. E **58**, 2796 (1998); **58**, 5586 (1998).
[10] A. Gorbatyuk and F.-J. Niedernostheide, Phys. Rev. B **59**, 13 157 (1999).
[11] N. A. Vlasenko, A. I. Beletskii, and A. E. Belyaev, in *Proceedings of the 23rd Conference on Physics of Semiconductors*, edited by M. Scheffle and R. Zimmermann (World Scientific, Singapore, 1996), Vol. 4, p. 2977.
[12] C. Radehaus, H. Willebrand, R. Dohmen, F.-J. Niedernostheide, G. Bengel, and H.-G. Purwins, Phys. Rev. A **45**, 2546 (1992).
[13] I. Müller, C. Punset, E. Ammelt, H.-G. Purwins, and J.-P. Boeuf, IEEE Trans. Plasma Sci. **27**, 20 (1999).
[14] I. Brauer, C. Punset, H.-G. Purwins, and J.-P. Boeuf, J. Appl. Phys. **85**, 7569 (1999).
[15] M. Or-Guil, E. Ammelt, F.-J. Niedernostheide, and H.-G. Purwins, Pitman Res. Notes Math. **335**, 223 (1995).
[16] C. P. Schenk, M. Or-Guil, M. Bode, and H.-G. Purwins, Phys. Rev. Lett. **78**, 3781 (1997).
[17] B. I. Datsko, Fiz. Tekh. Poluprovodn. **31**, 250 (1997) [Semiconductors **31**, 146 (1997)].
[18] M. Or-Guil, M. Bode, C. P. Schenk, and H.-G. Purwins, Phys. Rev. E **57**, 6432 (1998).
[19] W. Rühle, V. Marrello, and A. Onton, J. Electron. Mater. **8**, 839 (1979).
[20] B. Kukuk, S. Zuccaro, F.-J. Niedernostheide, and H.-G. Purwins, Acta Tech. CSAV **42**, 717 (1997).
[21] A. I. Beletskii and N. A. Vlasenko, Pis'ma Zh. Tekh. Fiz. **19**, 58 (1993) [Tech. Phys. Lett. **19**, 61 (1993)].
[22] F.-J. Niedernostheide, Ch. Gossen, and H.-G. Purwins, *Advances in Synergetics* (Belarussian State Univ. Press, Minsk, 1994), Vol. 2, p. 33.
[23] Ch. Gossen, F.-J. Niedernostheide, and H.-G. Purwins, Springer Proc. Phys. **79**, 112 (1995).
[24] H. Rüfer, V. Marrello, and A. Onton, J. Appl. Phys. **51**, 1163 (1980).
[25] M. I. J. Beale, J. Kirton, and M. Slater, Springer Proc. Phys. **38**, 296 (1989).
[26] A. I. Beletskii and N. A. Vlasenko, Pis'ma Zh. Tekh. Fiz. **19**, 33 (1993) [Tech. Phys. Lett. **19**, 13 (1993)].
[27] Y. Ono, H. Kawakami, M. Fuyama, and K. Onisawa, Jpn. J. Appl. Phys., Part 1 **26**, 1482 (1987).
[28] D. H. Smith, J. Lumin. **23**, 209 (1981).
[29] E. Bringuier, Philos. Mag. B **75**, 209 (1997).
[30] P. de Visschere and K. Neyts, J. Lumin. **92**, 313 (1992).
[31] W. Howard, O. Sahni, and P. M. Alt, J. Appl. Phys. **53**, 639 (1982).
[32] T. D. Thompson and J. W. Allen, J. Phys. C **20**, L499 (1987).
[33] M. I. J. Beale, Philos. Mag. B **68**, 573 (1993).
[34] G. Vincent, A. Chantre, and D. Bois, J. Appl. Phys. **50**, 5484 (1979).